Problem Sheet 12

Open Quantum Systems WS18-19

Iyán Méndez Veiga
iyan.mendez-veiga@uni-ulm.de

Code available here: https://github.com/iyanmv/OQS_ws18-19.

Exercise 26

a) Simulation of a two-site closed system with energy difference $\Delta\Omega = \Omega_1 - \Omega_2 = 0$ and electronic coupling $J = 100$. Perfect coherent energy transfer is observed since there is on interaction with the thermal bath. See Figure 1. Values are plotted from $t = 0$ to $t = 0.1$ so it is possible to observe the fast oscillations.

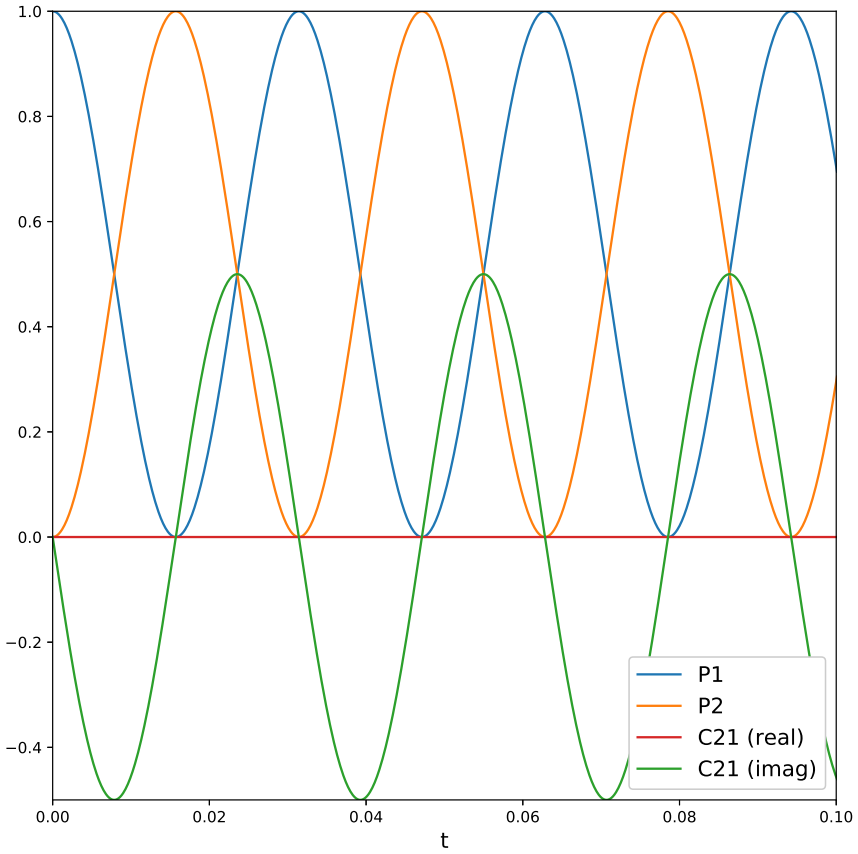

Figure 1: Obtained populations $P_1(t) = \langle 1|\,\rho_s(t)\,|1\rangle$ and $P_2(t) = \langle 2|\,\rho_s(t)\,|2\rangle$, and inter-site coherence $C_{21}(t) = \langle 2|\,\rho_s(t)\,|1\rangle$, using Runge-Kutta method from $t = 0$ to $t = 0.1$.

b) Same parameters as before but now with each site coupled to an independent thermal bath modelled with quantum harmonic oscillators for temperature $(k_B T/\hbar) = 100$. An Ohmic spectral density

$$\mathscr{J}_k(\omega) = \frac{2\lambda_k}{\pi}\frac{\omega\,\gamma_k}{\omega^2 + \gamma_k^2} \tag{1}$$

was used with $\lambda_k = 10$ and $\gamma_k = 50$. See Figure 2.

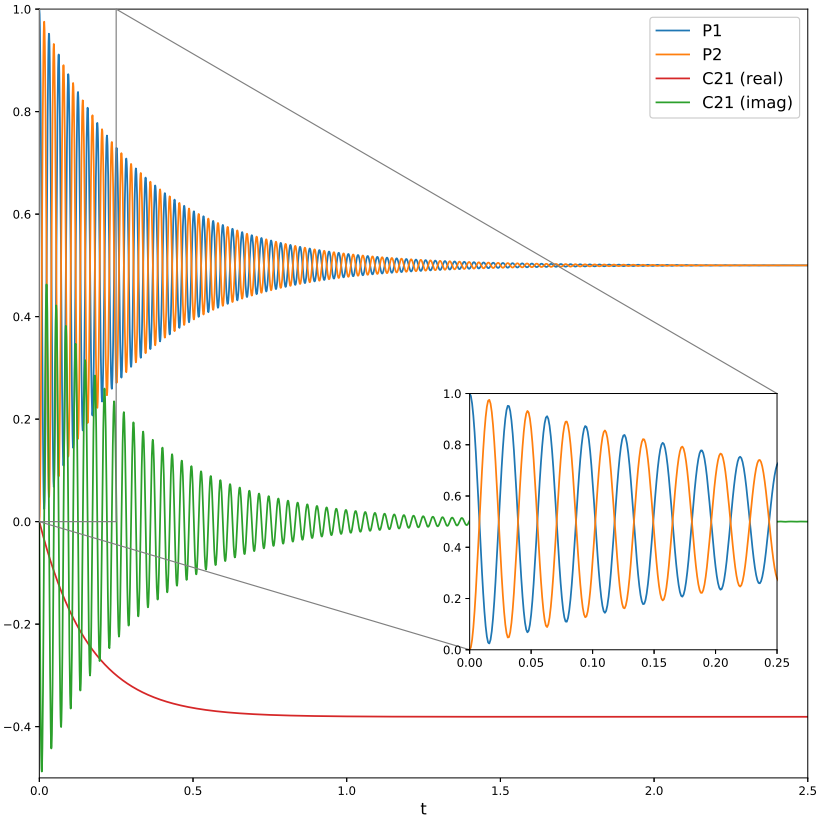

Figure 2: Obtained populations $P_1(t) = \langle 1| \rho_s(t) |1\rangle$ and $P_2(t) = \langle 2| \rho_s(t) |2\rangle$, and inter-site coherence $C_{21}(t) = \langle 2| \rho_s(t) |1\rangle$, using Runge-Kutta method from $t = 0$ to $t = 2.5$. It can be seen that $P_1(t) = P_2(t) = 0.5$ for long enough times because of $\Omega_1 = \Omega_2$.

c) Same parameters from **b)** but now with $\Delta\Omega = \Omega_1 - \Omega_2 = 100$. See Figure 3.

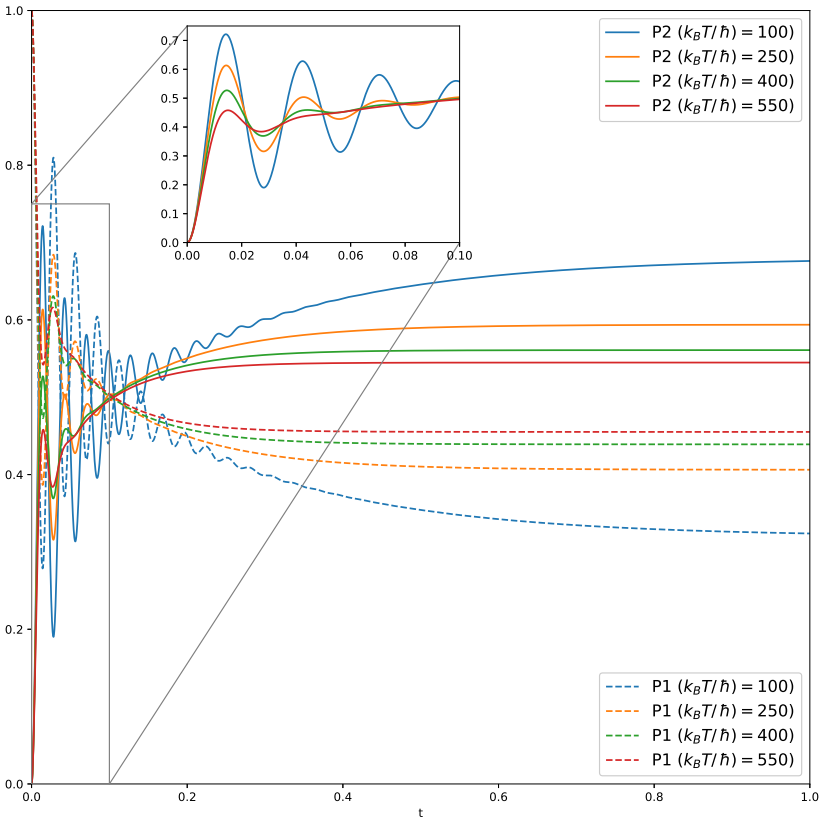

Figure 3: Populations $P_1(t) = \langle 1| \rho_s(t) |1\rangle$ and $P_2(t) = \langle 2| \rho_s(t) |2\rangle$ from $t = 0$ to $t = 1$. When saturated, $P_2^{(s)}$, becomes higher than $P_1^{(s)}$ because $\Omega_1 > \Omega_2$. This difference, $P_2^{(s)} - P_1^{(s)}$ is reduced when temperature increases.

d) The time evolution of the negativity of $\hat{\rho}_s(t)$ is simulated with the same parameters from **c)**, but now with a stronger environmental coupling $\lambda_k = 1000$. See Figure 4.

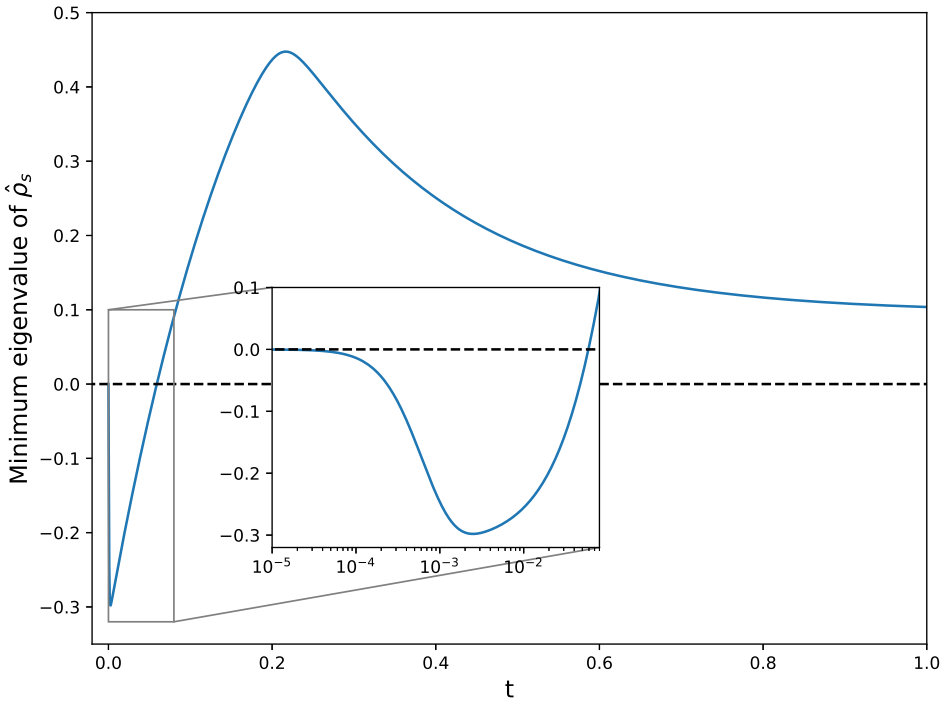

Figure 4: The minimum eigenvalue of $\hat{\rho}_s$ is plotted from $t = 0$ to $t = 1$. Negativity of $\hat{\rho}_s(t)$ can be observed at first with a minimum of ≈ -0.3 which is reached at $t \approx 2.5\,\mathrm{ms}$. After $t = 0.1$, the system $\hat{\rho}_s$ is positive semidefinite again.

e) With the same parameters from **d)**, the secular approximation is used to avoid the negativity. See Figures 5, 6 and 7

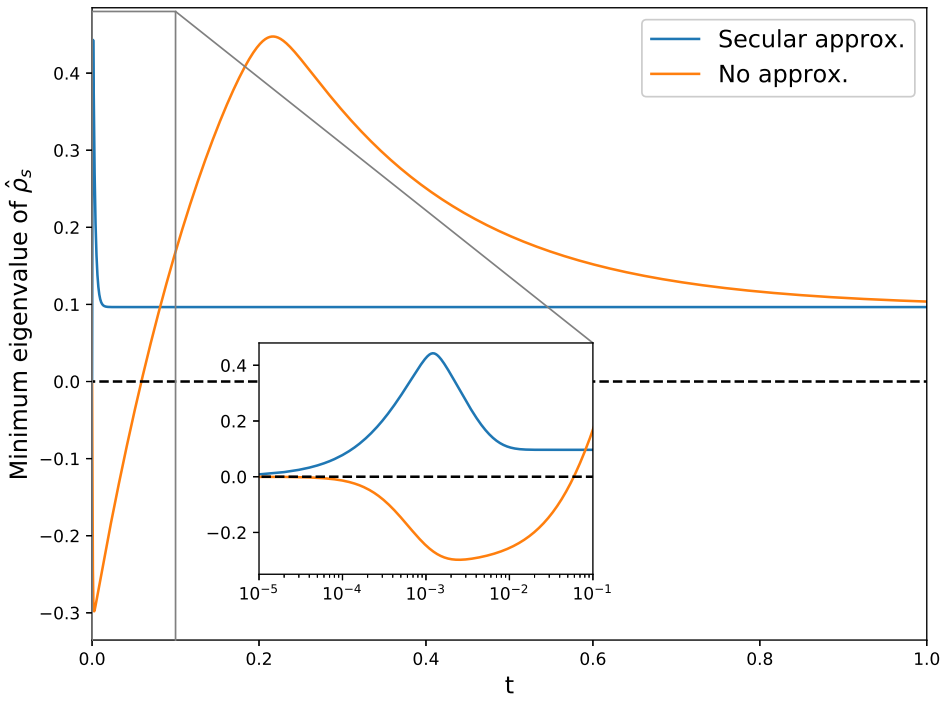

Figure 5: Negativity of $\hat{\rho}_s(t)$ from $t = 0$ to $t = 1$. When using the secular approximation (blue) the negativity disappears.

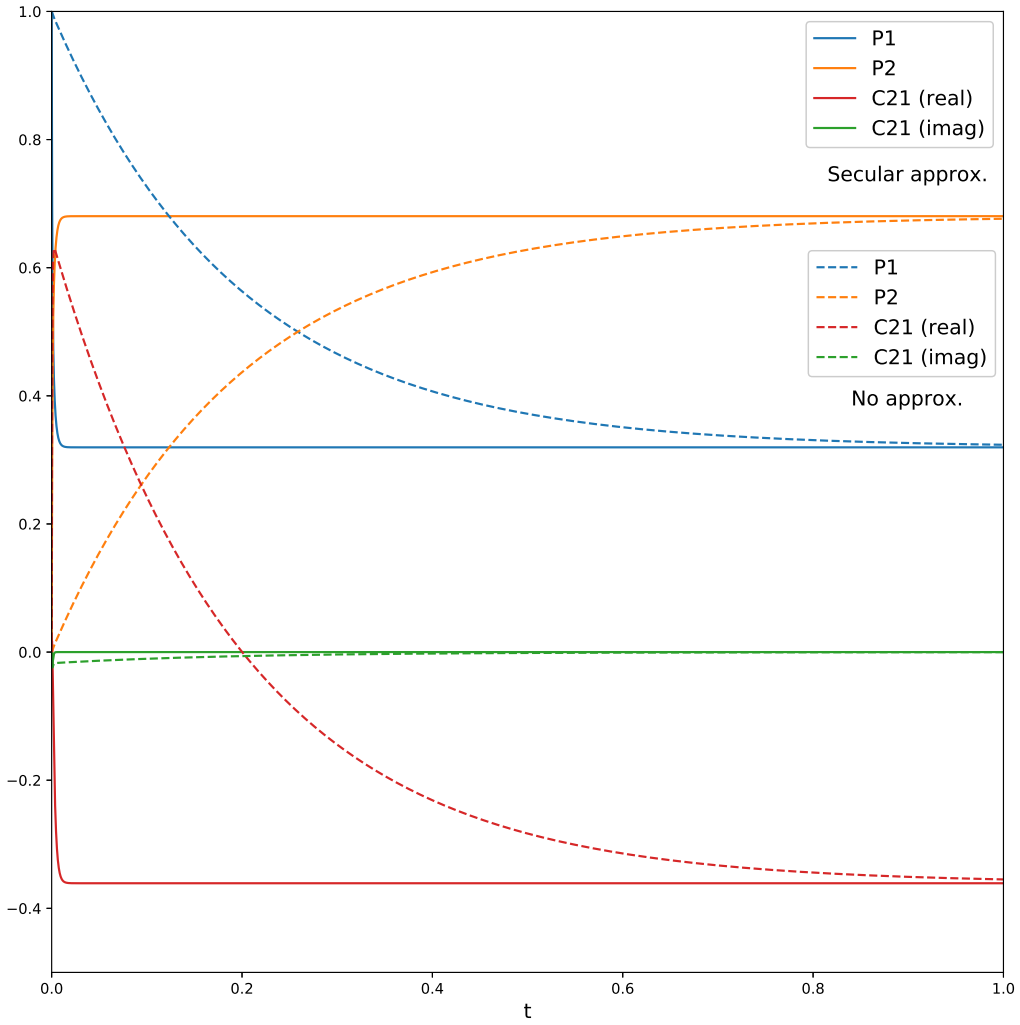

Figure 6: Time evolution of the populations and inter-site coherence using the secular approximation (solid lines) and without (dashed lines) from $t = 0$ to $t = 1$.

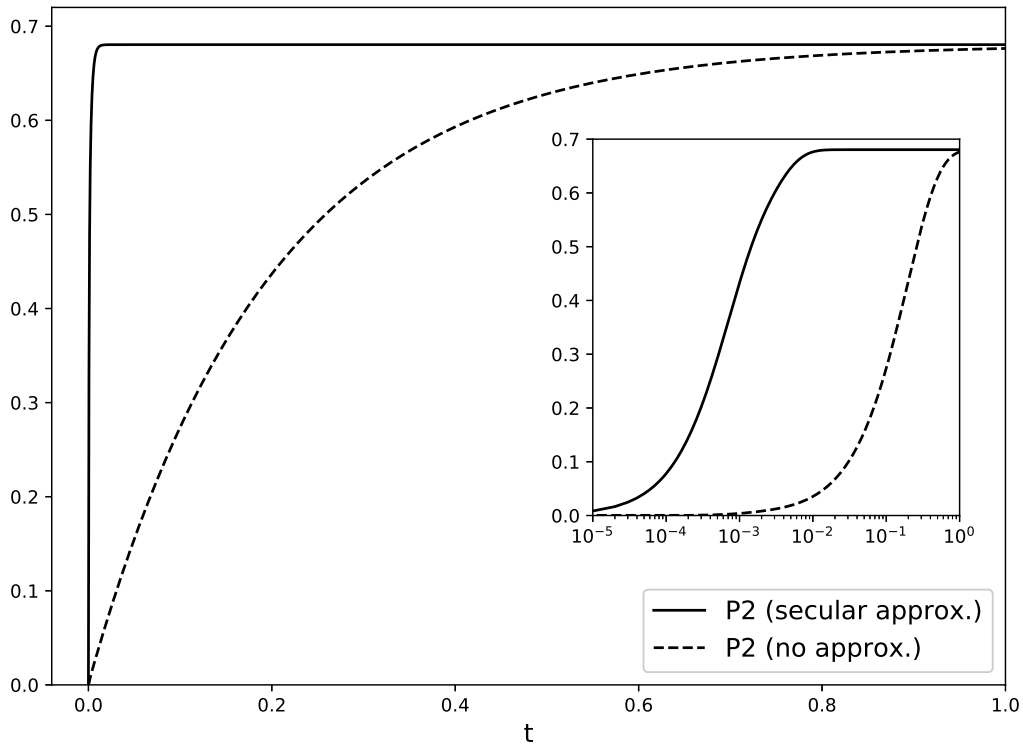

Figure 7: Time evolution of just the population of site 2 from $t = 0$ to $t = 1$.

f) For the last part, a moderate environmental coupling strength is consider ($J \approx \lambda_k$). This does not cause the negativity effect as before, but induces non-secular effects modulating system dynamics. See Figure 8.

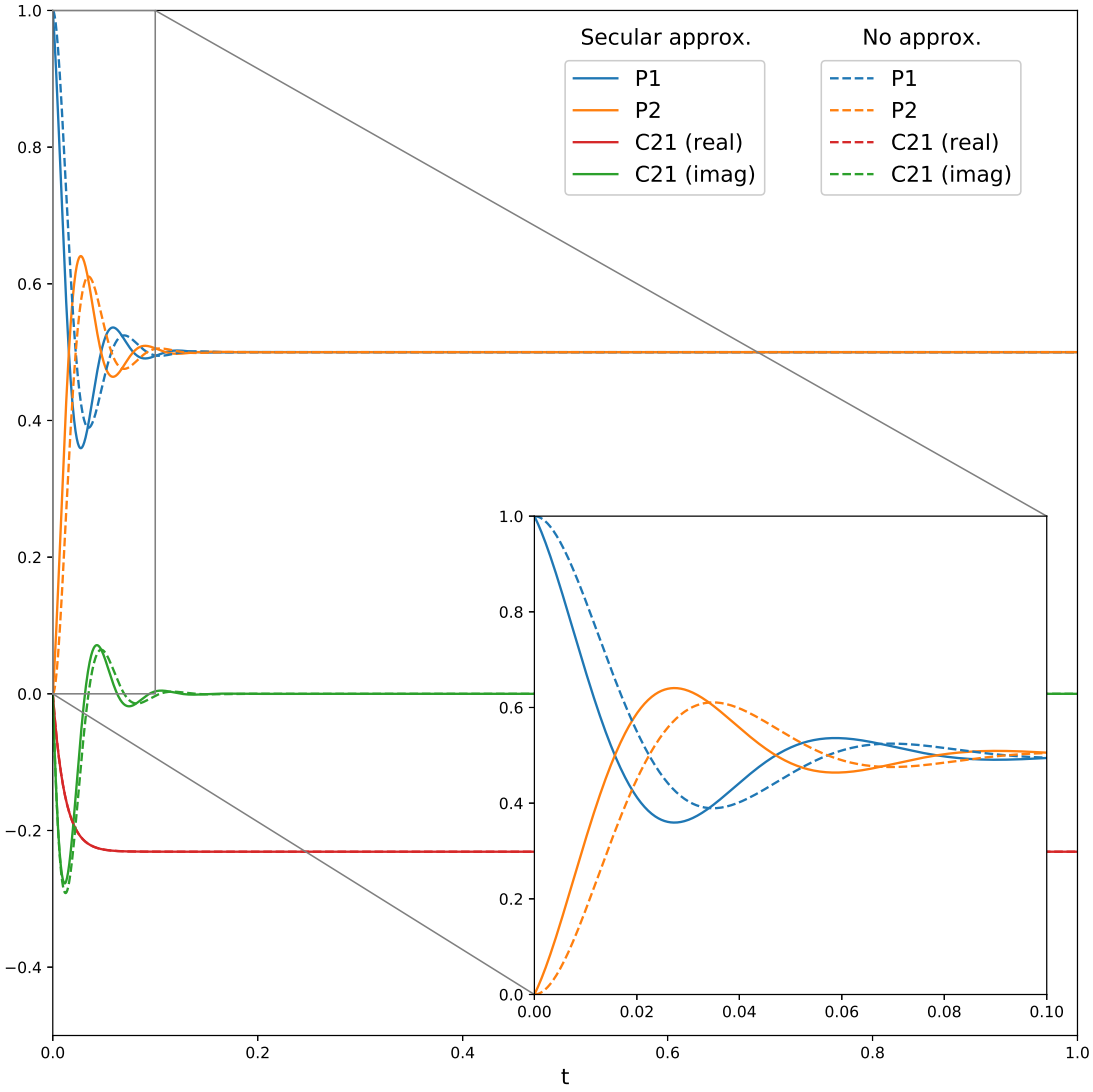

Figure 8: Time evolution of the site populations from $t = 0$ to $t = 1$. Non-secular effects can be observed before the saturation time ($t < 0.1$) in the zoomed area.